temperature and particle size. Experimental data showed that as the temperature increased from 10 to 28 °C, the microcrystal size (D 011) decreased from 139 to 80 nm, while the nanoparticle size decreased from 337 to 97 nm. This phenomenon is mainly attributed to the increased nucleation rate at higher temperatures. With the formation of more crystalline nuclei, the available reactants are distributed among more growing particles, resulting in smaller final particle sizes. Further innovation emerged from studying the effects of biomolecules on MOF formation. By incorporating proteins such as pepsin and lysozyme, researchers demonstrated that amino acid proton transfer ability and concentration directly influence the morphology and encapsulation efficiency of biomolecule-MOF composites. This study identified how proteins act as nucleation sites within amorphous MOF structures. These insights not only advance our understanding of biomineralization but also hint at designing proteins as nucleation sites for amorphous MOF growth.

In summary, this transdisciplinary research offers profound insights into the molecular mechanisms of biomimetic mineralization, where biological principles inspire synthetic material design. The findings pave the way for designing tailored MOF systems for applications. By bridging computational modeling simulations and experimental validation, this study provides a comprehensive "blueprint in a drop"—a molecular-level precision for understanding and optimizing MOF formation. By mastering these

microscopic processes, the team unlocks more sustainable and innovative applications in fields ranging from energy storage to pharmaceuticals. The journey from a single aqueous drop to a complex crystalline network underscores the profound potential of small beginnings in shaping the advanced materials of the future. (Reported by Hsiao-Ching Yang, Fu Jen Catholic University)

This report features the work of Hsiao-Ching Yang and her collaborators published in ACS Nano 18, 25170 (2024).

## TPS 13A Biological Small-angle X-ray Scattering

- In situ SWAXS
- Physical Chemistry, Chemical Physics, Computation Chemistry, Materials Science, Aqueous Chemistry

#### References

- S.-Y. Chen, W.-S. Lo, Y.-D. Huang, X. Si, F.-S. Liao, S.-W. Lin, B. P. Williams, T.-Q. Sun, H.-W. Lin, Y. An, T. Sun, Y. Ma, H.-C. Yang, L.-Y. Chou, F.-K. Shieh, C.-K. Tsung, Nano Lett. 20, 6630 (2020).
- P. K. Lam, T. H. Vo, J.-H. Chen, S.-W. Lin, C.-L. Kuo, J.-J. Liao, K.-Y. Chen, S.-R. Huang, D. Li, Y.-H. Chang, H.-Y. Chen, H.-T. Hsieh, Y.-A. Hsu, H.-K. Tsao, H.-C. Yang, F.-K. Shieh, J. Mater. Chem. A 11, 24678 (2023).
- 3. S.-W. Lin, P. K. Lam, C.-T. Wu, K.-H. Su, C.-F. Sung, S.-R. Huang, J.-W. Chang, O. Shih, Y.-Q. Yeh, T. H. Vo, H.-K. Tsao, H.-T. Hsieh, U-S. Jeng, F.-K. Shieh, H.-C. Yang, ACS nano 18, 25170 (2024).

# **Unlocking Hydrogen Power with Single-Atom Pt Catalysts**

3D hierarchically organized metal single atoms have attracted considerable attention for their high efficiency in various catalytic reactions.

Single-atom catalysts have garnered significant attention because of their exceptional activity and efficiency across a broad spectrum of catalytic reactions. However, developing stable single-atom catalysts and cocatalysts that maintain high performance presents significant challenges, particularly in achieving uniform dispersion, stabilization, and a sufficiently high density of single-atom sites. Currently, the majority of reported single-atom catalysts have predominantly been achieved using two-dimensional substrates lacking steric infrastructures. The dispersion of these single-atom catalysts relies heavily on their adsorption or coordination with substrates, such as carbon blacks or graphene surfaces. These weak interactions struggle to counteract the aggregation of single-atom catalysts into nanoparticles during catalytic reactions, leading to suboptimal performance.

Recent studies have suggested the potential use of metal–organic frameworks (MOFs) to create three-dimensional (3D) hierarchical structures, thus allowing the deployment of catalysts/cocatalysts inside MOF cages through diffusion or onsite reduction. This approach aims to mitigate the aggregation effect of single atoms, thereby sustaining their performance. However, achieving a uniform deposition of single catalysts/cocatalysts throughout the deep inner MOF cages presents a significant challenge.

U-Ser Jeng and his team at the NSRRC recently developed a method that involves embedding single platinum (Pt) atoms within silicate nanochannels for a paired single-atom cocatalyst and catalyst to achieve efficient and stable photocatalytic centers of a high number density in 3D substrates. Using phosphotungstic acids (PTAs) as templates, they achieved a high loading of single Pt atoms (3.0 wt%). Advanced techniques, including X-ray absorption spectroscopy (TPS 44A)<sup>2</sup> and electron microscopy, revealed that Pt atoms are stabilized via four-oxygen coordination within PTA, effectively reducing the energy-driving aggregation (Fig. 1). This system's design relies on controlling the ratio of Pt atoms to PTA. A critical ratio of 3.7 ensures nearly pure single-atom dispersion. At higher ratios, Pt clustering becomes evident. The research team used a three-stage solution synthesis process of template formation, Pt adsorption, and reduction at the air-liquid interface to create this unique structure. In situ grazing-incidence small-angle scattering (GISAXS) measurements (TLS 23A1 and TPS 13A)3,4 and thermogravimetric analyses demonstrated that increasing PTA content enhanced single-atom dispersion, while excessive PTA led to structural deterioration. The resulting Pt-PTA pairs within silicate nanochannels exhibit the outstanding hydrogen evolution reaction (HER) efficiency, achieving a hydrogen production rate of 300 mmol/h/g Pt, which is double that of previous systems. The PTA's empty tungsten d shell facilitates photoexcited electron transfer to Pt, enabling efficient hydrogen reduction. The nanochannels also prevent Pt clustering and sustain long-term performance. This breakthrough establishes a record-high Pt efficiency for HER among polyoxometalate (POM)-based systems. The 3D-ordered structure stabilizes single Pt atoms and creates a synergistic network for enhanced charge transfer. This innovative strategy highlights the potential for developing robust, high-performance single-atom catalysts for energy applications.

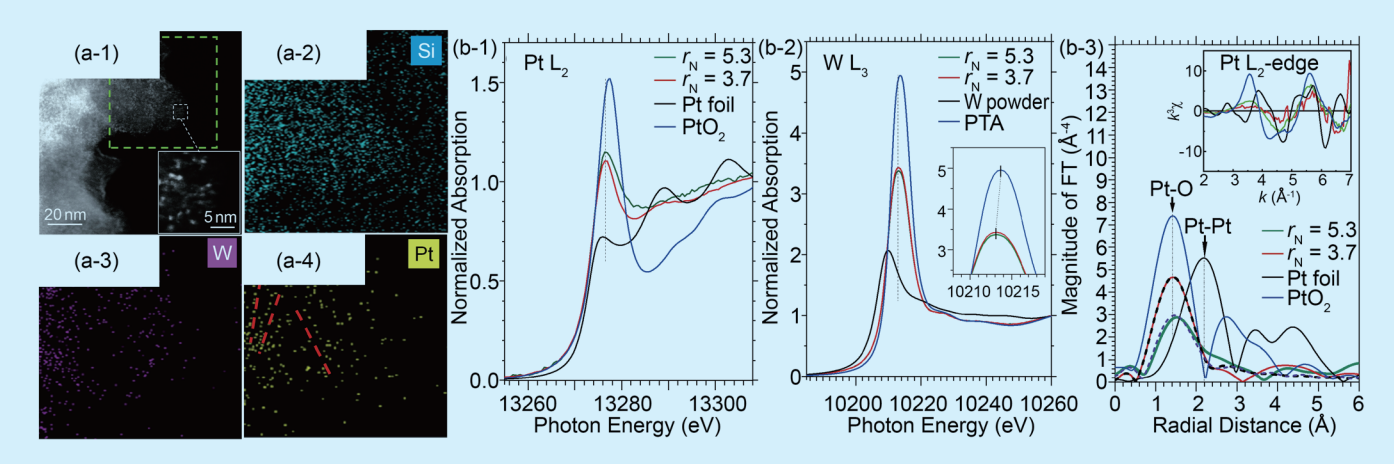


Fig. 1: (a-1) High-angle annular dark field-scanning transmission electron microscopy (HAADF–STEM) image of a typical zone on Pt–PTA within the silicate nanochannels of a low Pt atom/PTA number ratio,  $r_N$ , of 5.3; the inset (white square) zooms in on the local details, with the dispersed bright spots contributed by the scattering from heavier elements of Pt and W in the sample. Corresponding energy-dispersive X-ray spectroscopy (EDS) maps of (a-2) Si, (a-3) W, and (a-4) Pt, taken from the sample zone marked by the green dotted frame in (a-1). (b-1–3) X-ray absorption spectra measured at the (b-1) Pt L<sub>2</sub>-edge and (b-2) W L<sub>3</sub>-edge for the two samples of Pt–PTA within silicate nanochannels, with  $r_N$  = 5.3 and 3.7. Also shown are the spectra of Pt foil (measured in transmission mode), PtO<sub>2</sub>, and tungsten and PTA powders for comparison. (b-3) Fourier transform of the samples and the references (with no phase corrections). The inset shows the corresponding (same colors) Pt L<sub>2</sub>-edge k<sup>3</sup>-weight extended X-ray absorption fine structure (EXAFS) spectra. The data with  $r_N$  = 3.7 (or 5.3) are respectively fitted with the dotted (or dashed) curve by using a mean first-shell coordination number Nc = 3.88 (or 2.6) and a Pt–O bond length R = 1.93 Å (or 1.96 Å). [Reproduced from Ref. 5]

From the HER and X-ray absorption spectroscopy (XAS) results, Pt single atoms in  $Pt_1$ –PTA pair coordination within the arrayed silicate nanochannels outperform Pt nanoparticles with PTA in the same environment by fourfold efficiency (**Fig. 2(a)**, see next page). Such one-to-one  $Pt_1$ –PTA pair coordination has many advantages in the photoelectric conversion of HER *via* metal-to-metal charge-transfer excitation. In this process, the WO<sub>3</sub>-based PTA (having an empty d shell with tungsten W<sup>6+</sup> in  $5d^0$  configuration) provides photoexcited electrons, with the states of W<sup>5+</sup> in  $5d^1$  configuration to the coordinated  $Pt_1$  for hydrogen reduction. The PTA-4H site provides  $Pt_1$  a stable absorption and four coordinated oxygen atoms for an oxidation state of ca. +2 (as revealed from the XAS and discrete Fourier transform calculation results). The median oxidation state of  $Pt_1$  presumably is favorable for serving as a co-catalyst to accept photoelectrons from PTA and subsequently transfer the electrons to nearby protons for HER. The hydrogen adsorption energy  $Pt_1$  of  $Pt_2$  and subsequently transfer the electrons to nearby protons for HER. The hydrogen adsorption energy  $Pt_2$  faster, easier hydrogen desorption after reduction. These advantages render the  $Pt_1$  of the  $Pt_1$ -PTA pair an efficient co-catalyst in the photocatalytic HER mechanism. On top of the high HER efficiency within the  $Pt_1$ -PTA pair, the 3D network of a high number density of  $Pt_1$ -PTA pairs organized *via* the arrayed silicate nanochannels can further synergistically convert near neighbors' photoelectrons available within the network and those contributed by the PTA in the HER solution. Moreover, the nanochannel pore

structure (ca. 2 nm channel pore size) with densely intercalated PTA (ca. 1 nm size) suppresses the clustering of the channel  $Pt_1$  during catalytic reactions for sustainable performance. With all these advantages, this new hierarchical structure achieves a record high Pt efficiency in HER among the POM-based photocatalytic systems. It may be considered an efficient electrode material in photoelectrochemical cells.

In summary, the team successfully developed a three-stage synthesis process at the air-liquid interface, enabling precise control over the deposition and dispersion of platinum atoms (Pt<sub>1</sub>) within hexagonally packed

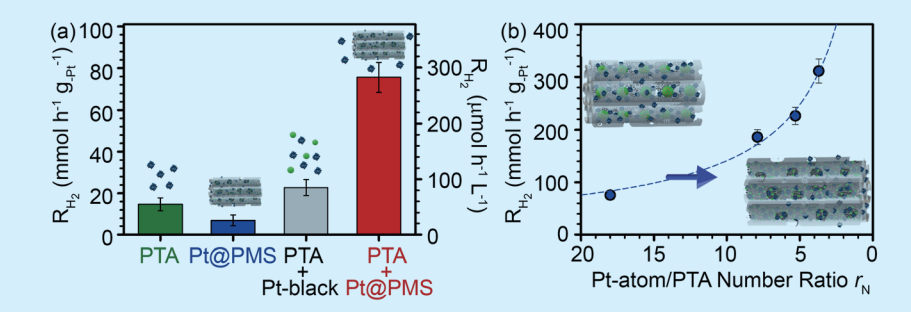


Fig. 2: (a) H<sub>2</sub> production rate measured for a 100 mL solution containing 5 mg of the nanocomposite of Pt–PTA within silicate nanochannels ( $r_N$  =18), 1.2 mM PTA, 0.2 M H<sub>2</sub>SO<sub>4</sub>, and isopropanol (20% vol.). Also shown are the H<sub>2</sub> production rates measured in similar solutions for the nanocomposite, solely PTA, and Pt black (of an equal Pt weight) suspension, in similar PTA solutions, as illustrated by the illustrations. (b) Increase in the H<sub>2</sub> production rate with the reduction of  $r_N$  of the nanocomposite with increasingly more Pt<sub>1</sub>–PTA pairs; inset illustrations show the corresponding transition of Pt dispersion from nanoparticles (left) to Pt<sub>1</sub> on PTA (right) within the arrayed silicate nanochannels. [Reproduced from Ref. 5]

silicate nanochannels. This approach achieved an efficient Pt<sub>1</sub>–PTA configuration, demonstrating record-high performance in HER. The outstanding performance of this structure is attributed to the stable 4H-site coordination, enhanced electron transfer efficiency, high-density Pt<sub>1</sub>–PTA pairs, and exceptional anti-clustering properties. Moreover, the integration of synchrotron radiation techniques, such as GISAXS and XAS, played a pivotal role in providing high-sensitivity *in situ* analysis, allowing a detailed understanding of the formation mechanism, structural characteristics, and reaction dynamics of Pt<sub>1</sub>–PTA pairs within the nanochannels. These advanced characterization methods offered critical data for the experimental process and provided valuable insights for designing and optimizing 3D single-atom catalysts. This study highlights the potential of combining synchrotron radiation capabilities with advanced synthesis techniques to develop highly stable and efficient single-atom catalysts. It paves the way for innovative applications in photochemical and renewable energy conversion systems. (Reported by Je-Wei Chang)

This report features the work of U-Ser Jeng and his collaborators published in ACS Nano 18, 1611 (2024).

# TPS 13A Biological Small-angle X-ray Scattering TPS 44A Quick-scanning X-ray Absorption Spectroscopy TLS 23A1 Small/Wide Angle X-ray Scattering

- GISAXS, NEXAFS, WAXS
- Materials Science, Chemistry, Surface, Interface and Thin-film Chemistry, Condensed-matter Physics

### References

- 1. X. F. Yang, A. Wang, B. Qiao, J. Li, J. Liu, T. Zhang, Acc. Chem. Res. 46, 1740 (2013).
- 2. C.-W. Pao, J. L. Chen, J. F. Lee, M. C. Che, C. Y. Huang, C. C. Chiu, C. Y. Chang, L. C. Chiang, Y. S. Huang, J. Synchrotron Radiat. 28, 930 (2021).
- 3. U.-S. Jeng, C. H. Su, C.-J. Su, K.-F. Liao, W.-T. Chuang, Y.-H. Lai, J.-W. Chang, Y.-J. Chen, Y.-S. Huang, M.-T. Lee, K.-L. Yu, J.-M. Lin, D.-G. Liu, C.-F. Chang, C.-Y. Liu, C.-H. Chang, K. S. Liang, J. Appl. Crystallogr. 43, 110 (2010).
- 4. O. Shih, K. F. Liao, Y. Q. Yeh, C. J. Su, C. A. Wang, J. W. Chang, W. R. Wu, C. C. Liang, C. Y. Lin, T. H. Lee, C. H. Chang, L. C. Chiang, C. F. Chang, D. G. Liu, M. H. Lee, C. Y. Liu, T. W. Hsu, B. Mansel, M. C. Ho, C. Y. Shu, F. Lee, E. Yen, T. C. Lin, U. Jeng, J. Appl. Crystallogr. 55, 340 (2022).
- 5. J. W. Chang, K. H. Su, C. W. Pao, J. J. Tsai, C. J. Su, J. L. Chen, L. M. Lyu, C. H. Kuo, A. C. Su, H. C. Yang, Y. H. Lai, U. S. Jeng, ACS Nano 18, 1611 (2024).